

# Novel Composite Polymer Electrolytes of PVdF-HFP Derived by Electrospinning with Enhanced Li-Ion Conductivities for Rechargeable Lithium–Sulfur Batteries

Pavithra M. Shanthi,<sup>†</sup> Prashanth J. Hanumantha,<sup>‡</sup> Taciana Albuquerque,<sup>§</sup> Bharat Gattu,<sup>†</sup> and Prashant N. Kumta<sup>\*,†,§,||,⊥</sup>

<sup>†</sup>Department of Chemical and Petroleum Engineering, University of Pittsburgh, Pittsburgh, Pennsylvania 15261, United States

<sup>‡</sup>Department of Bioengineering, University of Pittsburgh, Pittsburgh, Pennsylvania 15261, United States

<sup>§</sup>Department of Chemical Engineering, Arizona State University, Tempe, Arizona 85287, United States

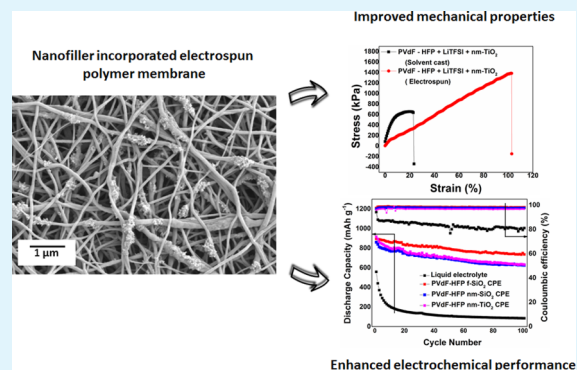
<sup>||</sup>Department of Mechanical Engineering and Materials Science, University of Pittsburgh, Pittsburgh, Pennsylvania 15261, United States

<sup>⊥</sup>Center for Complex Engineered Multifunctional Materials, University of Pittsburgh, Pittsburgh, Pennsylvania 15261, United States

## Supporting Information

**ABSTRACT:** Composites of poly(vinylidene fluoride-co-hexafluoro propylene) (PVdF-HFP) incorporating 10 wt % bis-(trifluoromethane)sulfonimide lithium salt (LiTFSI) and 10 wt % particles of nanoparticulate silica (nm-SiO<sub>2</sub>), nanoparticulate titania (nm-TiO<sub>2</sub>), and fumed silica (f-SiO<sub>2</sub>) were prepared by electrospinning. These membranes served as host matrix for the preparation of composite polymer electrolytes (CPEs) following activation with lithium sulfur battery electrolyte comprising 50/50 (vol %) dioxolane/dimethoxyethane with 1 M LiTFSI and 0.1 M LiNO<sub>3</sub>. The membranes consist of layers of fibers with average fiber diameter of 0.1–0.2 μm. CPEs with f-SiO<sub>2</sub> exhibited higher ionic conductivity with a maximum of  $1.3 \times 10^{-3}$  S cm<sup>-1</sup> at 25 °C obtained with 10 wt % filler compositions. The optimum CPE based on PVdF-HFP with 10 wt % f-SiO<sub>2</sub> exhibited enhanced charge–discharge performance in Li-S cells at room-temperature eliminating polysulfide migration, delivering initial specific capacity of 895 mAh g<sup>-1</sup> at 0.1 C-rate and a very low electrolyte/sulfur (E/S) ratios between 3:1 to 4:1 mL.g<sup>-1</sup>. The CPEs also exhibited very stable cycling behavior well over 100 cycles (fade rate ~ 0.056%/cycle), demonstrating their suitability for Li-S battery applications. In addition, the interconnected morphological features of PVdF-HFP result in superior mechanical properties (200–350% higher tensile strength). Higher Li-ion conductivity, higher liquid electrolyte uptake (>250%) with dimensional stability, lower interfacial resistance, and higher electrochemical stability are some of the attractive attributes witnessed with these CPEs. With these improved performance characteristics, the PVdF-HFP system is projected herein as suitable polymer electrolytes system for high-performance Li–S rechargeable batteries.

**KEYWORDS:** lithium–sulfur battery, composite polymer electrolyte, nanoparticle fillers, polymer membranes, low electrolyte (E)/sulfur (S) ratio, mechanical properties, electrochemical stability



## 1. INTRODUCTION

Lithium battery technology over the past 2 decades has witnessed unprecedented development due to the incessant increased demand for ever-increasing portable electronic devices and the all-pervading reality of hybrid electric vehicles. Portable electronic devices and the personal digital assistants (PDAs) in use today are already utilizing secondary lithium-ion batteries (LIBs),<sup>1,2</sup> which are as yet not economical for large-scale plug-in hybrid applications. In addition, there is an increasing concern associated with the safety of LIBs drawing considerable attention of researchers targeting the development

of high energy density, leak-free, and flexible lithium polymer batteries with improved safety.<sup>3,4</sup>

Though the field of LIBs has witnessed tremendous progress, transition metal oxide and phosphate-based systems are still the dominant archetypical systems used as cathodes exhibiting a maximum theoretical capacity of ~200–300 mA h/g.<sup>5,6</sup> This specific capacity limitation, along with the ensuing high costs

Received: November 3, 2017

Accepted: January 9, 2018

Published: January 9, 2018

and ecological concerns associated with these materials, restricts their application in large-scale devices.

Lithium–sulfur battery (Li–S) technology has in recent years been considered and widely investigated as a potential alternative and, more importantly, a much more economically favorable system that could realize expedient technology translation for use in current LIBs. The system also boasts superior theoretical capacity (1674 mA h/g) and specific energy density (2600 W h/kg)<sup>7</sup> of the cost-effective elemental sulfur in comparison with conventional cathode materials. In addition to the low cost, the large abundance and environmentally friendly attributes of sulfur make it a promising candidate cathode material for large-scale energy storage applications. However, lithium–sulfur batteries suffer from inefficient utilization of the active material due to the insulating nature of sulfur.<sup>8,9</sup> The lithium polysulfides formed during the electrochemical cycling of sulfur are highly soluble in organic liquid electrolytes leading to loss of active material which in turn results in poor cyclability.<sup>10,11</sup>

Improved active material utilization can be achieved by embedding the electrochemically active sulfur into a conducting carbonaceous<sup>12–15</sup> or polymer matrix forming composites.<sup>16–19</sup> This technique provides a conducting network for sulfur, hence improving the conductivity of the composite. Other approaches to improve the capacity of Li–S battery involve the use of chemical interactions of polysulfides with transition metal oxides<sup>20,21</sup> and trapping of sulfur into porous structures<sup>22–25</sup> preventing their dissolution. Though these approaches can increase the active material utilization of sulfur cathodes, they unfortunately, do not completely prevent the polysulfide species from dissolving into the electrolyte.<sup>26</sup>

Another approach to reduce the dissolution of sulfur is to modify the electrolyte by replacing it with an ionic liquid electrolyte,<sup>12,27–29</sup> polymer electrolyte,<sup>9,30–34</sup> or even Li-ion conducting solid electrolytes.<sup>35–38</sup> Among these approaches addressing modification of the electrolyte, replacing the liquid organic liquid electrolytes with polymeric electrolytes is certainly highly promising and has proven to be an effective approach.<sup>39</sup> In general, a polymer electrolyte may be defined as a membrane with transport properties similar to liquid ionic electrolytes.<sup>4,40</sup> Polymer electrolytes, originally developed for the lithium-ion battery system<sup>41–44</sup> could be modified for application in lithium–sulfur batteries. All the polymer systems are conveniently grouped into two broad categories, namely, solid polymer electrolytes (SPEs) and gel polymer electrolytes (GPEs).

Solid polymer electrolytes are composed of a lithium salt (e.g., LiPF<sub>6</sub>, LiCF<sub>3</sub>SO<sub>3</sub>, and LiC(CF<sub>3</sub>SO<sub>2</sub>)<sub>3</sub>) dissolved in high molecular weight polymers such as poly(ethylene oxide) (PEO) or poly(propylene oxide) (PPO), with the polymer acting as a solid solvent.<sup>45,46</sup> SPE conducts ions through local segment motion of polymer unfortunately, resulting in poor ionic conductivities. The second class of polymer electrolyte, GPE on the other hand, is obtained by incorporating liquid electrolyte into a polymer matrix that forms a stable gel polymeric host, resulting in high ionic conductivities.<sup>40,47</sup>

Other unique advantages of GPEs over liquid electrolyte include no internal short-circuiting and, moreover, allows minimal electrolyte leakage that is highly conducive to prevention of polysulfide dissolution, an inherent problem of Li–S batteries as outlined above.<sup>48–51</sup> The prerequisites of GPEs for lithium–sulfur batteries includes the following: high ionic conductivity at ambient and non-ambient temperatures,

high transference number,<sup>52</sup> good mechanical strength,<sup>49</sup> and good thermal and electrochemical stability as well as compatibility with electrodes.<sup>50,51</sup> In addition GPEs have the ability to act as a physical barrier to prevent the dissolution of polysulfide ions from the cathode and subsequently depositing at the anode.<sup>53</sup> Identification of an effective system combined with a suitable yet very effective fabrication process could catapult the system into being a highly attractive vehicle for translational implementation in commercial Li–S rechargeable battery systems.

An approach that is highly amenable for generation of GPE, electrospinning, is an efficient fabrication process that gives porous and fibrous membranes with average diameters ranging from 100 nm to 5  $\mu$ m,<sup>54</sup> which are at least 1 or 2 orders of magnitude smaller than the fibers produced from other fiber fabrication processes such as melt and solution spinning. Electrospinning technology has recently made strides into various fields such as preparation of porous filters, myriad biomedical scaffold and device materials, reinforcing components, cloths for electromagnetic wave shielding, sensors, and electronic devices, etc.<sup>55,56</sup> Electrospun mats of conventional polymer composites have also been used as electrolytes for lithium batteries.<sup>42,44,47,57,58</sup> These electrospun polymer electrolytes show superior mechanical and ionic properties due to their unique fibrous structure. However, to date, there are no known reports on using electrospun polymer membranes as electrolytes for lithium–sulfur batteries.

In the present study, poly(vinylidene fluoride-co-hexafluoro propylene) (PVdF-HFP) based CPEs (composite polymer electrolytes) were prepared by a simple electrospinning technique. Further, nanoparticulate SiO<sub>2</sub> (nm-SiO<sub>2</sub>) and TiO<sub>2</sub> (nm-TiO<sub>2</sub>) prepared using a simple sol–gel based nanofabrication technique<sup>59,60</sup> and commercially available fumed SiO<sub>2</sub>(f-SiO<sub>2</sub>) were also used as fillers to augment the mechanical and Li-ion conducting properties of these CPEs among other necessary ionic transport requirements. These nanofiller incorporated PVdF-HFP composite polymer electrolytes as separator–electrolytes were then tested to demonstrate their improved cycling stability using commercial sulfur as cathodes in Li–S batteries, the results of which are described and discussed in the present work.

## 2. EXPERIMENTAL SECTION

**2.1. Materials.** Polymer PVdF-HFP (MW  $\sim$  400,000, Aldrich), solvents *N,N*-dimethylformamide (DMF; ACS reagent,  $\geq$ 99.8%, Aldrich), acetone (ACS reagent,  $\geq$ 99.5%, Aldrich), and bis-(trifluoromethane)sulfonimide lithium salt (LiTFSI) (99.95% trace metals basis, Aldrich) used for the electrospinning process were vacuum-dried for 12 h at 60  $^{\circ}$ C before further use.

Commercially available f-SiO<sub>2</sub> (0.007  $\mu$ m powder, Aldrich) was used as-received in this work without any further treatment. Reagents for synthesizing nanometer-sized SiO<sub>2</sub> and nanometer-sized TiO<sub>2</sub> nanoparticles which include tetraethyl orthosilicate (TEOS; 99.99%, Aldrich), titanium(IV) isopropoxide (TTIP; 97%, Aldrich), ethanol (99.99%, Aldrich), 2-propanol (ACS reagent,  $\geq$ 99.5%, Aldrich), hydrochloric acid (ACS reagent, 37%, Aldrich), and ammonium hydroxide (ACS reagent, 28.0–30.0% NH<sub>3</sub> basis, Aldrich) were used without any further purification. Finally, Milli-Q water (18.2  $\Omega$ ) was used throughout the entire experiment.

**2.2. Preparation of PVdF-HFP Nanofiber Membrane.** The CPEs of PVdF-HFP (10 wt %) and LiTFSI (0.1 wt %) were prepared by dissolving the components in a mixed solvent of DMF/acetone (7:3, w/w) at 50  $^{\circ}$ C for 12 h until a homogeneous solution was formed. The resulting solution was dispersed with (0.1 wt %) nanofiller (nm-SiO<sub>2</sub>/nm-TiO<sub>2</sub>/f-SiO<sub>2</sub>) under sonication for 12 h. The

CPEs were prepared by a typical electrospinning method at room temperature. Electrospinning of the nanofiller dispersed solution was performed at a flow rate of 1 mL/h and a high voltage of 20 kV at room temperature with 15 cm distance maintained between the tip of the syringe and the rotating drum. The nanofibers deposited onto the rotating drum were then collected and dried under vacuum for 12 h at 60 °C at 1 atm. The nanofiber mats were then heat pressed at 80 °C for 30 min at 1 atm pressure and activated by soaking in 1.8 M LiTFSI and 1 M LiNO<sub>3</sub> in 1:1 (vol %) dioxolane/dimethoxyethane for 30 min before use as a separator–electrolyte complex in Li–S battery.

**2.3. Preparation of SiO<sub>2</sub> Nanoparticles.** The nanoparticles of SiO<sub>2</sub> were prepared by hydrolysis of TEOS in ethanol medium in the presence of ammonium hydroxide as reported by Rao et al.<sup>59</sup> Initially, 3 mL of TEOS was mixed with 20 mL of ethanol under sonication. A 20 mL aliquot of ammonium hydroxide solution (28–30%) was then added to this solution under sonication to promote the condensation reaction. The white turbid solution of SiO<sub>2</sub> nanoparticles was centrifuged and then dried under vacuum for 12 h. The SiO<sub>2</sub> nanoparticles were heated at 700 °C for 4 h to remove any carbon residues.

**2.4. Preparation of TiO<sub>2</sub> Nanoparticles.** The nanoparticles of TiO<sub>2</sub> were also similarly prepared by the hydrolysis of TTIP in propyl alcohol following the published method.<sup>61</sup> Accordingly, 5 mL of TTIP was dissolved in 10 mL of isopropyl alcohol, and then the solution was added dropwise into 40 mL of water containing 2.5 mL of HCl under sonication. The colloidal solution was then filtered and dried under vacuum for 12 h. The fine powders of TiO<sub>2</sub> obtained after drying were then calcined at 800 °C for 3 h.

**2.5. Materials Characterization and Electrochemical Measurements.** It is important to understand the nature of the nanoparticulate fillers and the electrospun CPE membranes to explain the observed cycling stability. Accordingly, to investigate the microstructure of the nanofillers and electrospun CPE membranes, scanning electron microscopy (SEM) analysis was conducted on a Philips XL30 machine operating at 20 kV. The crystal structures of the synthesized nm-TiO<sub>2</sub>, nm-SiO<sub>2</sub>, and f-SiO<sub>2</sub> nanoparticles were characterized by X-ray diffraction using Philips XPERT PRO system employing Cu K $\alpha$  ( $\lambda = 0.15406$  nm). The scans were recorded in the  $2\theta$  range of 10°–90°, at a constant current of 40 mA and voltage of 45 kV. The average particle sizes of nm-SiO<sub>2</sub> and nm-TiO<sub>2</sub> were determined by conducting dynamic light scattering (DLS) experiments in a Malvern Zetasizer Nano ZS90. Samples for the DLS experiment were prepared by dispersing in DI water (0.01 g/mL) after being wetted in isopropanol to determine the average particle size. The nature of chemical bonding in the CPEs was further analyzed by attenuated total reflectance Fourier transform infrared spectroscopy (ATR-FTIR; Nicolet 6700 spectrophotometer, Thermo Electron Corp.) using a diamond ATR Smart orbit. Spectra were obtained at 1 cm<sup>-1</sup> resolution averaging 64 scans in the 400–4000 cm<sup>-1</sup> frequency range. The surface chemistry of the CPEs was probed by X-ray photoelectron spectroscopy (XPS) using an ESCALAB 250 Xi system (Thermo Scientific) equipped with a monochromated Al K $\alpha$  X-ray source. Beams of low-energy ( $\leq 10$  eV) Ar<sup>+</sup> ions and low-energy electrons guided by a magnetic lens were used to provide uniform charge neutralization. The standard analysis spot of 400  $\times$  400  $\mu\text{m}^2$  was defined by the microfocused X-ray source. The measurements were performed at room temperature in an ultrahigh-vacuum (UHV) chamber with the base pressure  $< 5 \times 10^{-10}$  mbar (the charge neutralization device produced  $2 \times 10^{-10}$  mbar partial pressure of Ar during measurements). The Advantage software package (Thermo Fisher Scientific) was used to fit the elemental spectra based on calibrated analyzer transmission functions, Scofield sensitivity factors, and effective attenuation lengths for photoelectrons from the standard TPP-2 M (Tanuma Powell and Penn -2M) formalism. The mechanical properties of the CPEs also need to be evaluated in order to explain the improved electrochemical performance of the CPEs. Accordingly, the stress–strain behavior of the polymer membranes was studied using an Instron universal tensile tester, Model 1123. The pore characteristics and specific surface area (SSA) of the nanofiller samples were analyzed on a Micromeritics ASAP 2020 physisorption analyzer,

using the Brunauer–Emmett–Teller (BET) isotherm generated. The powders were first vacuum degassed and then tested for nitrogen adsorption and desorption for the specific surface area analysis.

**2.6. Electrochemical Characterization.** Electrodes for battery half-cell characterization were prepared by casting a slurry of 70 wt % commercial sulfur, 20 wt % acetylene black, and 10 wt % PVdF in *N*-methylpyrrolidone (NMP) onto aluminum foil followed by drying under vacuum for 24 h. A uniform electrode sulfur loading varying between 1.5 and 2 mg cm<sup>-2</sup> was utilized for all the electrochemical measurements. 2025-type coin cells were assembled in an Innovative, Inc. glovebox (UHP argon,  $< 0.1$  ppm O<sub>2</sub>, and H<sub>2</sub>O) utilizing a slurry coating approach. Accordingly, sulfur electrodes formed the working electrode, lithium foil as the counter electrode, and the electrospun CPE membranes soaked in liquid electrolyte (1:1 (vol %) 1,3-dioxolane and 1,2-dimethoxyethane with 1.8 M LiTFSI and 0.1 M LiNO<sub>3</sub>) as the electrolyte/separator complex. The E/S ratios used in the CPE membranes were between 3:1 and 4:1 (mL g<sup>-1</sup>). Control samples were prepared under identical conditions replacing the CPE with 100  $\mu\text{L}$  of liquid electrolyte and Celgard 2400 polypropylene (PP) membrane as the separator. The E/S ratio in the control samples was maintained between 50:1 and 65:1 (mL g<sup>-1</sup>). The electrochemical cycling behavior of the cells thus prepared was studied by cycling between 1.7 and 2.6 V (with respect to Li<sup>+</sup>/Li) at 0.1 C ( $\sim 162$  mA/g) current rate using an Arbin BT200 battery testing system. Ionic conductivity of CPEs was studied using AC impedance spectroscopy in a Gamry potentiostat. The polymer membranes were accordingly secured between two steel disks, and data were collected in the high-frequency range (10–100 kHz). Equivalent circuit modeling was performed using the Z-view 2.0 (Scribner Associates Inc.) to obtain the CPE ionic conductivity values.

### 3. RESULTS AND DISCUSSION

**3.1. SEM Analysis of Nanofiller Particles.** Figure 1 shows the morphologies of nm-SiO<sub>2</sub>, nm-TiO<sub>2</sub>, and f-SiO<sub>2</sub> nanoparticles studied using SEM. nm-SiO<sub>2</sub> and nm-TiO<sub>2</sub> (Figure 1a,b) were observed to be spherical with a uniform particle size distribution similar to the observations reported in the reference method followed.<sup>59</sup> The nm-SiO<sub>2</sub> nanoparticles had

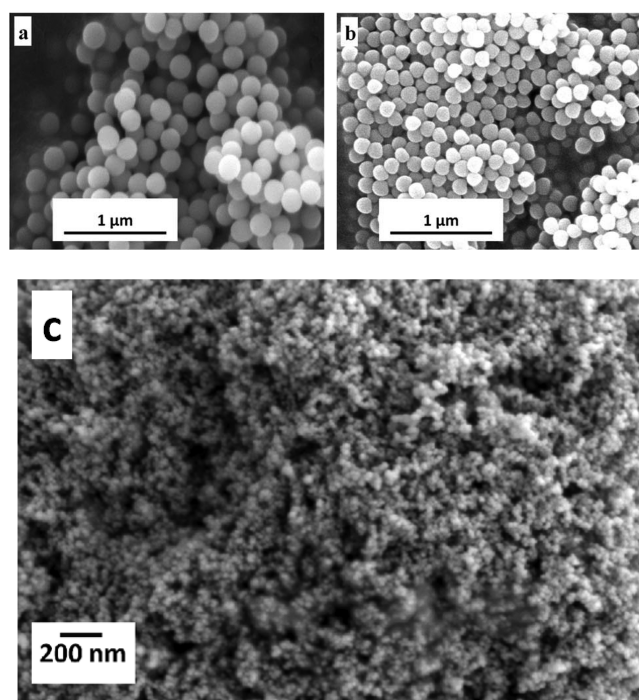


Figure 1. SEM images of (a) nm-SiO<sub>2</sub>, (b) nm-TiO<sub>2</sub>, and (c) f-SiO<sub>2</sub>.

**Table 1.** BET Surface Area Analysis of nm-SiO<sub>2</sub>, nm-SiO<sub>2</sub>, and f-SiO<sub>2</sub><sup>a</sup>

sample	BET surface area (m <sup>2</sup> /g)	Langmuir surface area (m <sup>2</sup> /g)	total pore vol (cm <sup>3</sup> /g)	adsorption av pore width (nm)
f-SiO <sub>2</sub>	191.61 ± 7.23	329.19 ± 9.14	0.42 ± 0.06	8.72 ± 1.04
nm-SiO <sub>2</sub>	18.03 ± 1.16	22.36 ± 1.92	0.21 ± 0.02	7.96 ± 0.92
nm-TiO <sub>2</sub>	6.47 ± 0.72	10.18 ± 0.65	0.17 ± 0.03	10.90 ± 0.75
Celgard 2400	46.42 ± 3.54	52.62 ± 6.91	0.12 ± 0.01	24.64 ± 1.62
electrospun PVdF-HFP	63.56 ± 2.34	71.92 ± 5.68	0.18 ± 0.03	14.24 ± 0.56
PVdF-HFP + f-SiO <sub>2</sub>	217.20 ± 6.25	342.5 ± 11.68	0.53 ± 0.06	14.42 ± 0.86
PVdF-HFP + nm-SiO <sub>2</sub>	99.04 ± 5.83	100.02 ± 6.98	0.25 ± 0.04	15.20 ± 0.49
PVdF-HFP + nm-TiO <sub>2</sub>	72.60 ± 3.76	86.50 ± 5.63	0.21 ± 0.03	12.20 ± 0.21

<sup>a</sup>Each datum represents an average of three independent tests run on three different samples under identical conditions.

an average particle diameter of ~200 nm which was further confirmed by DLS technique. The nm-TiO<sub>2</sub> particles were almost spherical shaped with ~150 nm diameter. The SEM of f-SiO<sub>2</sub> was performed at a higher magnification (Figure 1c), showing agglomerates of nanometer-sized individual particles. This is similar to the observations made by Zhou et al.<sup>62</sup> confirming the extremely small (~7 nm) particle size of f-SiO<sub>2</sub> mentioned in the product specification (Sigma-Aldrich, Inc.). The XRD patterns obtained from both nm-SiO<sub>2</sub> and f-SiO<sub>2</sub> showed patterns that correspond to amorphous structures, indicating the amorphous nature of both the SiO<sub>2</sub> samples. However, the XRD pattern of TiO<sub>2</sub> showed crystalline peaks corresponding to the anatase phase and crystal structure (Supporting Information Figure S1).

**3.2. Specific Surface Area Analysis.** Specific surface area of the nanofillers is an important factor deciding the electrochemical performance of the CPEs. It has been observed that smaller size particles for a similar volume fraction of the ceramic filler phase would impart an improved performance as compared to larger size particles because of their ability to cover more surface area.<sup>63</sup> The BET surface area analysis of the nanofillers is presented in Table 1.

The BET surface area results indicate that f-SiO<sub>2</sub> has a high BET surface area of 191.61 m<sup>2</sup>/g which is closer to the value (175–225 m<sup>2</sup>/g) from the product specifications. f-SiO<sub>2</sub> also exhibits a high pore volume of 0.417 cm<sup>3</sup>/g. On the other hand, nm-SiO<sub>2</sub> and nm-TiO<sub>2</sub> showed lower surface areas of 18.03 and 6.47 m<sup>2</sup>/g, respectively. The very high surface area of f-SiO<sub>2</sub> is expected to improve the performance of CPEs over other fillers. Table 1 also shows the specific surface areas and porosities of nm-SiO<sub>2</sub>, f-SiO<sub>2</sub>, and nm-TiO<sub>2</sub> incorporated PVdF-HFP hybrid membranes. For comparison, the porosity of a commercial polypropylene (PP) membrane separator (Celgard 2400) is also shown. The BET surface area of the polypropylene membrane is 46.42 m<sup>2</sup>/g comparable to the values reported in the literature.<sup>64,65</sup> The porosities of these hybrid membranes are significantly greater than that of microporous PP membrane. The PVdF-HFP nanofibers form free-standing nonwoven membranes that have relatively high porosities. The introduction of nm-SiO<sub>2</sub> and nm-TiO<sub>2</sub> nanoparticles further increases the porosity values due to the extra surface area of the nanoparticles. However, owing to the very high surface area of f-SiO<sub>2</sub> the BET surface area of f-SiO<sub>2</sub> incorporated PVdF-HFP membrane was found to be 217.2 m<sup>2</sup>/g, almost twice higher than that of the other nanofiller counterparts.

**3.3. SEM Analysis of the Nanofibers.** The electrospun polymer mats are usually required to be of uniform fiber thickness with a bubble-free morphology to serve as effective battery separators for use in battery applications.<sup>43</sup> Formation of bubble-like structures usually results in nonuniform pore

distribution in the mats and a decrease in the nanofiller exposure on the surface.<sup>66</sup> To understand the morphological characteristics of the membranes, the electrospun polymer mats were analyzed using the scanning electron microscopy technique. The SEM micrographs of PVdF-HFP membranes with 10 wt % dissolved LiTFSI (Figure 2a) show an

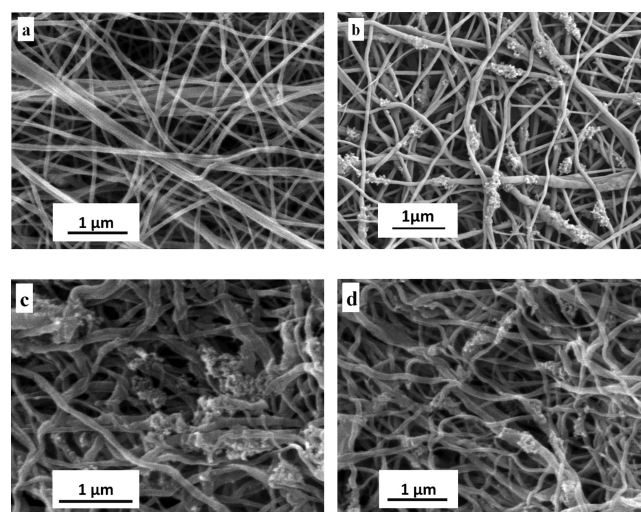


**Figure 2.** SEM images of (a) electrospun PVdF-HFP polymer membranes with dissolved LiTFSI, (b) electrospun PVdF-HFP with dissolved LiTFSI (10 wt %) and dispersed f-SiO<sub>2</sub> (10 wt %), (c) electrospun PVdF-HFP with dissolved LiTFSI (10 wt %) and dispersed nm-SiO<sub>2</sub> (10 wt %), and (d) electrospun PVdF-HFP with dissolved LiTFSI (10 wt %) and dispersed nm-TiO<sub>2</sub> (10 wt %).

interpenetrated fibrous network possibly resulting in an improvement in the mechanical strength of the CPEs. The membranes also exhibit a uniform and bead free morphology with fibers of ~175 nm diameter. SEM images of PVdF-HFP + LiTFSI membranes with dispersed 10 wt % f-SiO<sub>2</sub> (Figure 2b) indicate that the introduction of nanofillers does not change the morphology of the electrospun PVdF nanofibers. The nanoparticles of f-SiO<sub>2</sub> (~7 nm) are both embedded inside the nanofibers and dispersed on the fiber surface which is clearly observed in the SEM EDS mapping of the filler incorporated polymer mats (Figure S2), similar to the observations of Sethupathy et al.<sup>67</sup> in their reported studies on SiO<sub>2</sub> incorporated electrospun PVdF-HFP membranes. However, with PVdF-HFP + LiTFSI membranes containing 10 wt % nm-SiO<sub>2</sub> and nm-TiO<sub>2</sub> nanofillers, the surface of the membranes (Figure 2c,d) appears to show larger aggregates of the nanofiller particles. This is mainly attributed to the larger particle sizes of nm-SiO<sub>2</sub> (~200 nm) and nm-TiO<sub>2</sub> (~150 nm),

respectively, in comparison with f-SiO<sub>2</sub> (~7 nm). Correspondingly, the small particle size of f-SiO<sub>2</sub> renders it more amenable to being uniformly distributed; as a result, the SEM image correspondingly shows the matt morphology with the f-SiO<sub>2</sub> nanoparticles more uniformly dispersed and integrated into the surface structure. The surface roughness increased upon introduction of nanofillers, while the average diameter of nanofibers was largely unaffected. The exposure of nm-TiO<sub>2</sub>, nm-SiO<sub>2</sub>, and f-SiO<sub>2</sub> nanofillers on the fiber surfaces results in increasing the accessible surface area and forms extensive Lewis acid/base interactions with the ionic species in the liquid electrolyte possibly resulting in higher ionic conductivities.<sup>68</sup>

Solarajan et al. studied the effect of SiO<sub>2</sub> nanofiller composition on the surface morphology, electrolyte uptake, membrane porosity, and ionic conductivity.<sup>69</sup> Their study indicates that the ionic conductivity and electrolyte uptake of the polymer membranes increases with nanofiller concentration, decreasing steadily beyond 10 wt % SiO<sub>2</sub> composition. Similar observations were made by Stephan et al. and Angiah et al. in their studies on the effect of aluminum oxyhydroxide, (AlO[OH])<sub>n</sub>,<sup>70</sup> and ZrO<sub>2</sub>,<sup>71</sup> respectively. Accordingly, in order to obtain high electrolyte uptake, membrane porosity, and ionic conductivity, considering the results of the above explained researchers, a nanofiller composition of 10 wt % of the selected nanofillers (f-SiO<sub>2</sub>, nm-SiO<sub>2</sub>, and nm-TiO<sub>2</sub>) was also used in this study.

**3.4. FTIR Analysis.** Any change in the chemical nature of PVDF-HFP membranes upon addition of LiTFSI salt and nanofillers (f-SiO<sub>2</sub>, nm-SiO<sub>2</sub>, and nm-TiO<sub>2</sub>) needs to be understood in order to predict the chemical stability of the CPEs during electrochemical cycling.<sup>72</sup> The nature of the chemical bonding in PVDF-HFP and LiTFSI (Figure 3 and

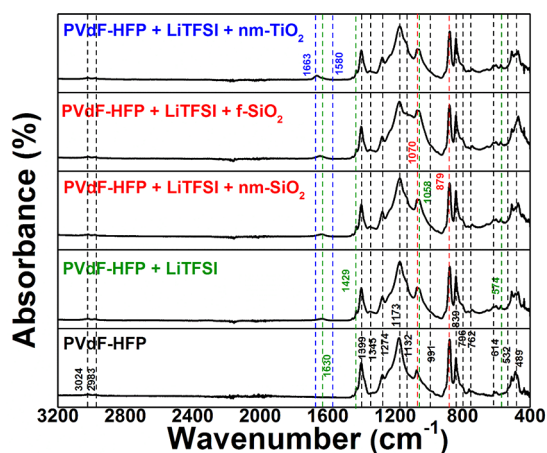


**Figure 3.** FTIR spectra of pure PVDF-HFP, PVDF-HFP with 10 wt % LiTFSI, and various nanofillers (10 wt %).

Figure S3) was accordingly analyzed using FTIR spectroscopy for comparison with LiTFSI incorporated polymer membranes. With PVDF-HFP being a semicrystalline polymer, the FTIR spectra of pure PVDF-HFP contains some crystalline ( $\alpha$ -phase) and amorphous ( $\beta$ -phase) phase related peaks. The bands of pure polymer PVDF-HFP due to the crystalline phase ( $\alpha$ -phase) are observed at 489, 532, 614, 762, 796, and 976 cm<sup>-1</sup>, while the bands related to the amorphous phase ( $\beta$ -phase) are observed at 839 and 879 cm<sup>-1</sup>,<sup>143</sup> which are individually indexed and explained in Table S1.

Addition of LiTFSI to the PVDF-HFP membranes introduces three distinct peaks at 1058, 1630, and 574 cm<sup>-1</sup><sup>143</sup> in the FTIR spectrum, in addition to the peaks corresponding to PVDF-HFP polymer. These observations exactly overlap with the findings of Shalu et al. related to the FTIR analysis of the interaction of LiTFSI with PVDF-HFP<sup>43</sup> according to which the peaks at 1058 and 574 cm<sup>-1</sup> are due to the asymmetric -S-N-S- stretching of LiTFSI and asymmetric CF<sub>3</sub> bending vibrations of LiTFSI salt, respectively. Furthermore, the peak at 1630 cm<sup>-1</sup> is due to the complexation between the polymer backbone and LiTFSI salt. The retention of all the characteristic peaks of PVDF-HFP even upon addition of LiTFSI indicates the absence of any form of chemical reaction between the polymer and the salt.

Comparing the spectra of PVDF-HFP before and after incorporation of the nanofillers (Figure 3), the intensity of the broad band centered at 1070 cm<sup>-1</sup> clearly increases for SiO<sub>2</sub> incorporated PVDF-HFP using the C-F symmetric stretching band at 879 cm<sup>-1</sup> as reference.<sup>73</sup> This is due to the overlap of the band from the F-C-F symmetric stretching vibration at 1072 cm<sup>-1</sup> and the band from the Si-O-Si antisymmetric stretching vibration at 1070 cm<sup>-1</sup>,<sup>74</sup> indicating the binding of Si-O- to the polymer.

In the case of the PVDF-HFP membranes incorporated with TiO<sub>2</sub>, the NH<sub>2</sub> group usually observed at 1600 cm<sup>-1</sup> is shifted to the lower wavenumber around 1580 cm<sup>-1</sup>.<sup>75</sup> In addition, the peak at 1663 cm<sup>-1</sup> becomes prominent due to enhanced -C=O stretching owing to the interaction with TiO<sub>2</sub>.<sup>76</sup> This indicates the fact that a greater number of ions coordinate with -NH<sub>2</sub>. The new interaction of the nanofiller, -TiO<sub>2</sub> and TiO<sub>2</sub>-polymer in the FTIR spectra of PVDF-HFP hybrid membranes, can be expected to improve the ionic conductivity of the system on the fiber surface.

**3.5. Mechanical Properties.** The mechanical properties of the electrospun polymer membranes are very important for effective application in batteries as separators. In the electrospun membranes, mechanical properties are expected to be improved due to entanglement of singular fibers aided by the presence of nanoparticle fillers.<sup>44</sup> The mechanical properties of the electrospun membranes were compared with those of solution cast membranes of the same composition to demonstrate the superior properties attained by the electrospinning method. The thickness of both electrospun and solvent cast membranes used for mechanical property measurements was maintained uniformly at 0.035 ± 0.005 mm. The strain vs stress and tensile strength of the hybrid membranes characterized by tensile measurements are represented in Figure 4a. Both the solvent cast and electrospun samples exhibited a linear elastic behavior comparable to the results from similar systems reported in literature.<sup>72,77</sup> The tensile strength of the electrospun membranes is uniformly superior to that of solvent cast membranes due to the enhanced elastic nature of the electrospun membranes as explained by Blond et al. on his work comparing the mechanical properties of electrospun and solvent cast membranes.<sup>78</sup> For example, the tensile strength increased from 650.73 MPa for solvent cast PVDF-HFP + LiTFSI + nm-TiO<sub>2</sub> membrane to 1409.92 MPa for electrospun membranes (Figure 4b), confirming the effect of electrospinning on improving the tensile properties of the hybrid membranes.

In addition to the improved mechanical properties, the flame retarding ability of the CPEs is an important factor that determines the safety of the lithium-ion battery.<sup>79,80</sup> CPEs

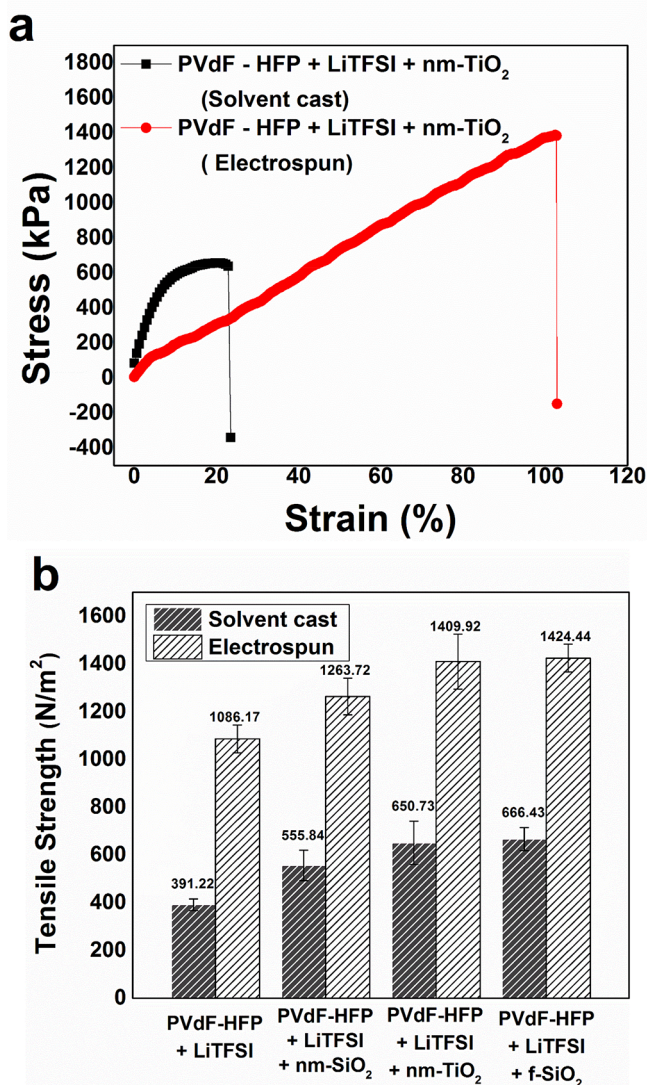


**Figure 4.** (a) Stress vs strain relationship of nm-TiO<sub>2</sub> incorporated membranes and (b) comparison of tensile strengths of various electrospun and solvent cast membranes. Each datum represents an average of three independent tests run on three different samples under identical conditions.

soaked in electrolyte were, thus, subjected to a combustion test by exposing them to heat for 60 s. Commercial Celgard 2400 PP separators soaked in electrolyte were also exposed to the same conditions, the results of which are shown in Figure S4. The commercial separator shrunk immediately after exposure to the flame. However, the CPEs remained unaffected by the heat exposure generated by the flame for more than 60 s and

the dimensions of the CPE membranes also remained unaltered, confirming the absence of shrinkage due to the high-temperature exposure generated from the flame. These results show that the CPE membranes show better flame retarding properties and thermal stability, which would subsequently make them a safer alternative for use in lieu of commercial separators and electrolytes.

**3.6. Electrolyte Uptake.** Figure S5 represents the relationship of electrolyte uptake of the nanofiber membranes with time, obtained by soaking the nanofiber membranes in the liquid electrolyte of 1.8 M LiTFSI and 0.1 M LiNO<sub>3</sub> in 1:1 (vol %) dioxolane and dimethoxyethane for a period of 30 min. The electrolyte uptake is observed to stabilize within the initial 10 min of exposure to electrolyte of all the hybrid polymer membranes.<sup>81</sup> The electrolyte uptake of f-SiO<sub>2</sub> membranes is ~219%, which is about four times higher than the uptake of commercial PP separator which is ~63%.<sup>82</sup> As expected, the higher pore volume of the f-SiO<sub>2</sub> material (Table 1) results in the highest electrolyte uptake for the same (Table 2). Though the electrolyte uptake of these membranes were high, the E/S ratio in these membranes was considerably low, ranging between 3:1 and 4:1 mL g<sup>-1</sup>. The high retention ability and faster penetration of liquid electrolyte into the fibrous membranes are due to the unique pores generated from the interconnected fibers, which in turn increase the ionic conductivity. PVDF-HFP + LiTFSI membranes showed a very high uptake value of ~550%, due to uncontrolled swelling of the membranes and lack of mechanical integrity owing to the absence of filler particles.

**3.7. Ionic Conductivity Studies.** The most important requirement of CPEs is their room-temperature Li-ion conductivity which needs to be closer to liquid electrolytes to display better electrochemical properties for potential applications in Li-ion batteries. EIS analysis of the CPEs was performed using stainless steel blocking electrodes on both sides. Nyquist plots of the EIS analysis of CPEs are shown in Figure 5a,b. The impedance plots were modeled to the general equivalent circuit using Z-view 2.0, shown in Figure 5c,<sup>83</sup> where  $R_s$  represents the electrolyte resistance and  $C_{dl}$  represents the capacitive coupling between the ionic conduction in the electrolyte and the electronic conduction in the measuring circuit. Additionally,  $C_g$  is the geometrical capacitance representing the capacitive effects of the cell hardware and of the electrical leads.<sup>84</sup> The electrolyte conductivity was, thus, calculated using  $R_s$ , thickness of the polymer membrane ( $t$ ), and the surface area of the electrolyte sample ( $A$ ) using the equation given as follows:

$$\sigma = \frac{t}{R_s A}$$

**Table 2. Electrolyte Uptake Studies on the Polymer Membranes<sup>a</sup>**

sample	electrolyte uptake (%)		
	after 10 min	after 30 min	after 60 min
PVdF-HFP + LiTFSI	436.6 ± 10.2	550 ± 11.3	551.5 ± 14.3
PVdF-HFP + LiTFSI + nm-SiO <sub>2</sub>	182.5 ± 7.8	190.5 ± 8.6	190.5 ± 9.2
PVdF-HFP + LiTFSI + f-SiO <sub>2</sub>	207.5 ± 13.4	219 ± 14.9	220 ± 10.7
PVdF-HFP + LiTFSI + nm-TiO <sub>2</sub>	253.5 ± 6.2	266.5 ± 9.6	270 ± 7.6
commercial PP separator	59.5 ± 2.5	63 ± 4.1	63 ± 2.7

<sup>a</sup>Each datum represents an average of three independent tests run on three different samples under identical conditions.

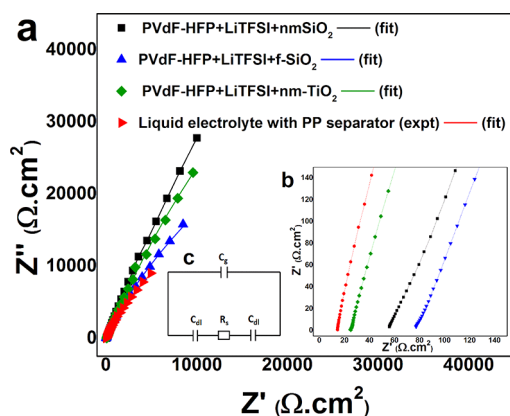


**Figure 5.** (a) Fitted Nyquist plot of the polymer membranes, (b) enlarged Nyquist plot (inset), and (c) equivalent circuit used to fit the Nyquist plots (inset).

The room-temperature conductivities of the polymer electrolytes are about  $\sim 10^{-3} \text{ S cm}^{-1}$  which is in line with several reports.<sup>4,40,50,51,85</sup> From the conductivity value of the electrolyte, it is seen that there is an increase in ionic conductivity of the CPE systems in comparison with the liquid electrolyte based separator. This is due to the enhanced electrolyte uptake due to the nanoporous structure of the electrospun membranes. The PVdF-HFP membranes with nm-SiO<sub>2</sub> fillers show the highest room-temperature conductivity of  $9.48 \times 10^{-3} \text{ S cm}^{-1}$  (Table 3). This is slightly unexpected due to the higher uptake

**Table 3.** Ionic Conductivity of Commercial Electrolyte and Various Polymer Membrane Electrolytes<sup>a</sup>

sample composition	conductivity ( $\text{S cm}^{-1}$ )
commercial separator with liquid electrolyte	$1.283 \pm 0.26 \times 10^{-3}$
PVdF-HFP + LiTFSI + nm-TiO <sub>2</sub>	$1.881 \pm 0.14 \times 10^{-3}$
PVdF-HFP + LiTFSI + f-SiO <sub>2</sub>	$3.009 \pm 1.65 \times 10^{-3}$
PVdF-HFP + LiTFSI + nm-SiO <sub>2</sub>	$9.48 \pm 0.87 \times 10^{-3}$

<sup>a</sup>Each datum represents an average of three independent tests run on three different samples under identical conditions.

seen in the case of f-SiO<sub>2</sub> indicating that ionic conductivity in the composite polymer electrolytes depends not only on the electrolyte uptake (Figure S5) and pore volume (Table 1) but also on the nature of the bonding of filler particles with the liquid electrolyte. Further studies are indeed warranted to obtain a good understanding of this unique phenomenon.

**3.8. Electrochemical Cycling Performance.** The electrochemical performance of the PVdF-HFP composite polymer electrolytes were studied by performing electrochemical charge–discharge cycling against commercial sulfur cathodes. The electrochemical cycling performance and Coulombic efficiencies of the polymer electrolytes are shown in Figure 6a. The PVdF-HFP-f-SiO<sub>2</sub> hybrid polymer separator shows an initial capacity of  $895 \text{ mAh g}^{-1}$  and a stable capacity of  $845 \text{ mAh g}^{-1}$  after 100 cycles (fade rate, 0.055%/cycle). On the other hand, PVdF-HFP-nm-SiO<sub>2</sub> shows an initial discharge capacity of  $860 \text{ mAh g}^{-1}$  which stabilizes at  $734 \text{ mAh g}^{-1}$  after 100 cycles (0.146%/cycle). The PVdF-HFP-nm-TiO<sub>2</sub> separators showed an initial capacity of  $915 \text{ mAh g}^{-1}$  and stabilized at  $749 \text{ mAh g}^{-1}$  (0.18%/cycle). Accordingly, all the CPEs exhibited average Coulombic efficiencies of 98–99%, indicating the absence of capacity loss due to polysulfide dissolution. However, the cells containing the commercial separator along

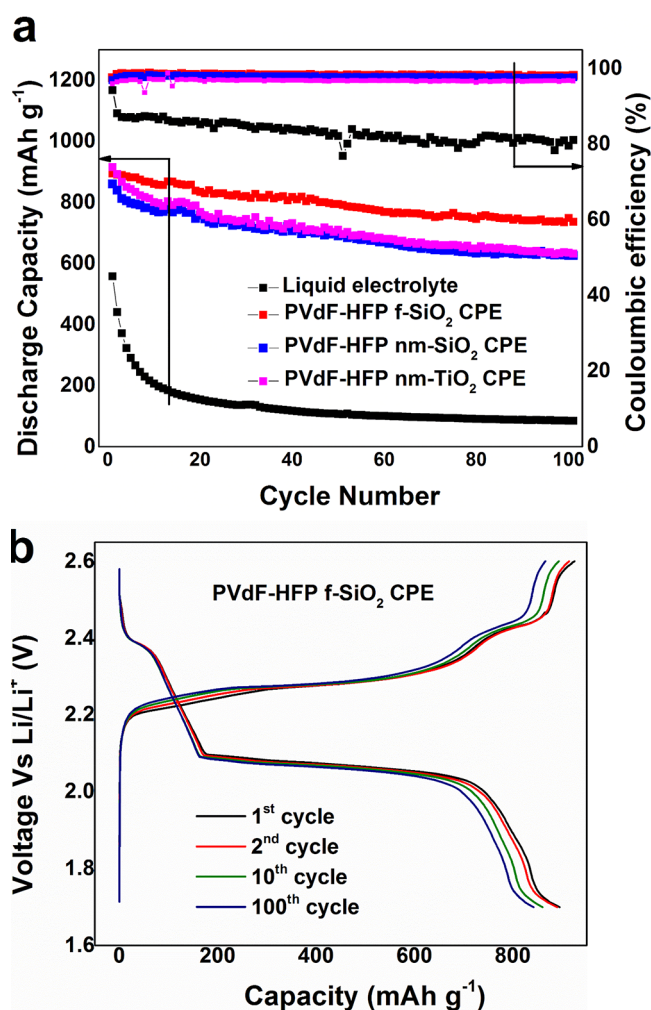


**Figure 6.** (a) Electrochemical cycle performance and Coulombic efficiencies of the different polymer membranes and (b) charge–discharge profile of PVdF-HFP + LiTFSI + f-SiO<sub>2</sub> polymer membrane.

with liquid electrolyte cycled opposite commercial sulfur cathode gave an initial capacity of  $557 \text{ mAh g}^{-1}$  which quickly faded to  $132 \text{ mAh g}^{-1}$  in less than 10 cycles. The commercial separator containing cells exhibit an initial Coulombic efficiency of 94.6% which quickly fades to 80% within the first 50 cycles, clearly indicating the presence of polysulfide dissolution resulting in loss in capacity and Coulombic efficiency. The charge–discharge profiles of the cell with PVdF-HFP + LiTFSI + f-SiO<sub>2</sub> CPE membrane is also shown in Figure 6b. The charge–discharge profiles of the other two CPE membranes are shown in Figure S6a,b. The voltage profiles of all the CPEs at first, second, 10<sup>th</sup>, and 100<sup>th</sup> cycles feature the two characteristic discharge plateaus; the plateau at around 2.4 V corresponds to the transformation from the S<sub>8</sub> molecular forms of the polysulfide to a series of soluble polysulfides. On the other hand, the plateau at 2.1 V corresponds to the transformation of the Li<sub>2</sub>S<sub>4</sub> species to insoluble Li<sub>2</sub>S<sub>2</sub> and Li<sub>2</sub>S.<sup>86,87</sup> The enhanced electrochemical cycling performance of the f-SiO<sub>2</sub> incorporated CPE is attributed to the higher surface area and pore volume of the filler particles that facilitated the formation of an insulated layer of ceramic particles at the electrode surface serving to impede electrode reactions as explained by Kumar et al.<sup>63</sup> This phenomenon has been observed by Capuano et al. when excessive amounts of the

passive ceramic phase were introduced into the polymer matrix.<sup>88</sup> This insulation layer, in addition to impeding surface reactions, facilitates prevention of polysulfide dissolution in Li–S battery, which explains the superior performance of the f-SiO<sub>2</sub> CPE over other fillers.

**3.9. XPS Analysis of Separators Postcycling.** X-ray photoelectron spectroscopy (XPS) analysis was performed on the polymer electrolyte separators after 100 cycles to understand the origin of the cycling stability of the hybrid polymer membranes. XPS was performed on both the side facing the sulfur cathode and the side facing lithium anode. Figure 7 represents the XPS of the polymer electrolyte

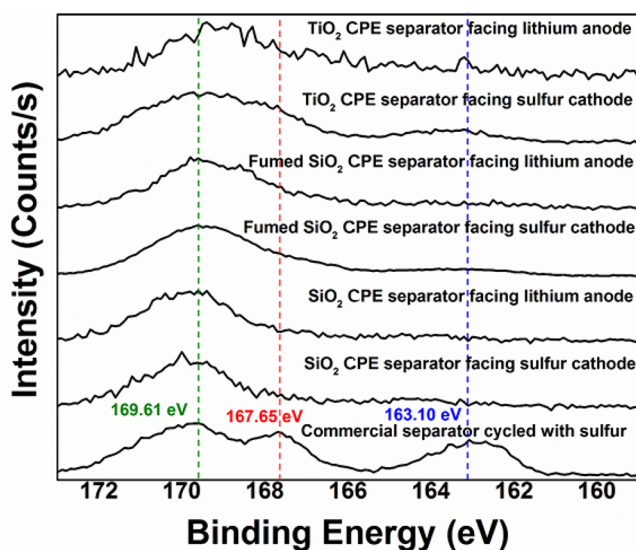


Figure 7. S 2p spectra of different separators before and after cycling.

membranes postcycling. The peak at 169.61 eV represents a S 2p peak corresponding to sulfur binding in LiTFSI; the peaks at 167.65 and 163.10 eV correspond to the higher order polysulfide and Li<sub>2</sub>S, respectively. Commercial separator and liquid electrolyte cycled with sulfur cathodes shows peaks corresponding to both higher and lower order polysulfide confirming polysulfide dissolution in the liquid electrolyte system. However, it should be noted that these polysulfide peaks are absent in polymer electrolyte membranes facing lithium anode, confirming the absence of polysulfide dissolution into the electrolyte. On the other hand, the side of the fumed SiO<sub>2</sub> and TiO<sub>2</sub> incorporated polymer membrane facing the sulfur cathode shows a very mild peak at 163.1 eV corresponding to Li<sub>2</sub>S. This might be due to the surface adsorbed Li<sub>2</sub>S molecules and not the dissolution of polysulfide.

**3.10. FTIR Analysis Postcycling.** It is well-known that the structural and chemical stabilities of the polymer membranes are two important parameters that decide the long-time performance of polymer electrolytes. The XPS analysis of the CPE membranes after electrochemical cycling provided information about the binding energy changes on the surface of the membranes. To ascertain the changes in chemical properties occurring in the bulk of the membrane and to confirm the absence of polysulfides, FTIR analysis was performed on the membrane surface facing the lithium anode and the surface facing the sulfur cathode. Accordingly, the FTIR spectrum of PVdF-HFP + LiTFSI + SiO<sub>2</sub> separator (activated by soaking in 1.8 M LiTFSI and 1 M LiNO<sub>3</sub> in 1:1 (vol %) dioxolane and dimethoxyethane for 30 min) before and after

100 charge–discharge cycles is shown in Figure 8. Similar studies on the f-SiO<sub>2</sub> and TiO<sub>2</sub> incorporated membranes showed identical results and are correspondingly tabulated in Table S2.

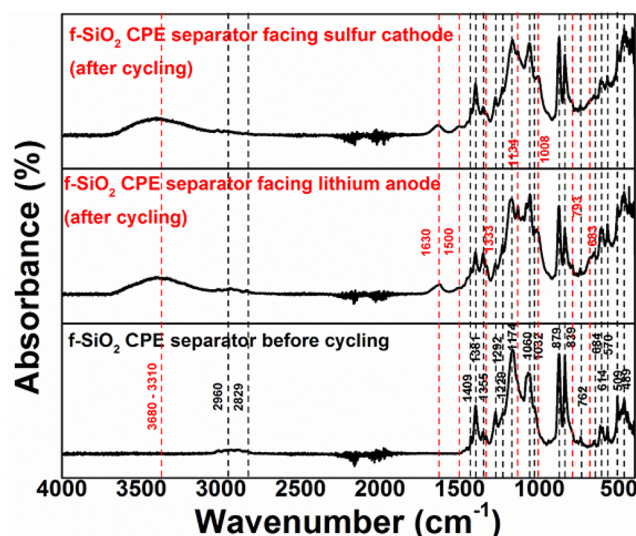


Figure 8. FTIR spectra of the SiO<sub>2</sub> polymer electrolyte membrane before and after 100 cycles (side exposed to lithium anode and sulfur cathode).

The FTIR spectrum of PVdF-HFP + LiTFSI + SiO<sub>2</sub> membrane soaked in electrolyte shows peaks corresponding to PVdF-HFP as explained in Table S2. In addition, the peaks at 1032 and 1070 cm<sup>-1</sup> correspond to the introduction of SO<sub>3</sub><sup>-</sup> group and overlap of F–C–F symmetric stretching vibrations and Si–O–Si asymmetric stretching vibrations resulting from LiTFSI and SiO<sub>2</sub>, respectively.<sup>89</sup> In addition, the spectrum for the polymer membranes collected prior to cycling shows peaks at 509, 570, 684, 762, 1229, 1355, 2829, and 2960 cm<sup>-1</sup>. These peaks correspond to the out of plane -C–C- bending of the ring structure of dioxolane,<sup>90</sup> symmetric deformation mode of -CF<sub>3</sub> group from interaction with dioxolane,<sup>91</sup> -N-H bending vibrations from the imide group of LiTFSI, -C=O vibrations (ester),<sup>92</sup> -C–N- stretching vibration,<sup>93</sup> -CH<sub>3</sub> vibration from dimethoxyethane, -CH<sub>2</sub> symmetric stretching vibrations,<sup>94</sup> and -C–H stretching vibrations, respectively.

After 100 charge–discharge cycles, both sides of the polymer membrane showed almost the same pattern with peaks at 3130–3680 cm<sup>-1</sup> indicating the presence of exchangeable protons, from the amide group of LiTFSI. The peaks at 1630 and 1500 cm<sup>-1</sup> correspond to -C=O bond from the carbonyl group of dimethoxyethane. The band around 1333 cm<sup>-1</sup> corresponds to the -C–H ring bending vibrations of dioxolane ring.<sup>95</sup> The peak at 1134 cm<sup>-1</sup> corresponds to stretching vibrations of the carbonate group.<sup>96</sup> The peaks at 1008, 793, and 683 cm<sup>-1</sup> correspond to -Si–O stretching vibrations,<sup>97</sup> the -SO<sub>3</sub> group from LiTFSI,<sup>98</sup> and Si–O–Si stretching vibration modes,<sup>99</sup> respectively. Polysulfide peaks arising due to -S–S- stretching vibrations usually occurring between 500 and 540 cm<sup>-1</sup>.<sup>100,101</sup> The absence of these peaks indicates the absence of dissolved polysulfide in the CPE membranes after cycling, thus confirming the results from XPS. The absence of any anomalous peaks further confirms the chemical stability of the polymer membranes even after prolonged cycling. The

chemical stability of the CPEs suggests their potential to replace PP separators in commercial sulfur batteries.

#### 4. CONCLUSIONS

In this work, f-SiO<sub>2</sub>, nm-SiO<sub>2</sub>, and nm-TiO<sub>2</sub> incorporated novel electrospun PVdF-HFP CPEs were tested as electrolytes in Li–S battery. The 10 wt % f-SiO<sub>2</sub> CPE exhibited an initial discharge capacity of 895 mAh g<sup>-1</sup> and very low fade rate of 0.055%/cycle when cycled for over 100 cycles at 0.1 C rate against commercial sulfur cathode. The study also conclusively indicates that the electrospinning technique improves the mechanical properties of the CPEs which in turn help suppress dendrite formation on the lithium anode. The nanofiller incorporated CPEs also exhibit excellent room-temperature ionic conductivity of  $9.48 \times 10^{-3}$  S cm<sup>-1</sup>, with values comparable to that of liquid electrolytes. The CPEs also exhibit excellent chemical stability upon cycling for over 100 cycles, confirmed using FTIR and XPS analysis. The study also highlights the advantage of high surface area f-SiO<sub>2</sub> filler in preventing polysulfide dissolution by forming an insulating film over the cathode. This has been confirmed using XPS analysis, which indicates the absence of polysulfide species on the surface of cycled separators. Polysulfide shuttling is usually observed in Li–S cells containing liquid electrolytes and commercial separators. In contrast, the CPE membrane described herein can suppress the dissolution and migration of the polysulfides generated and deposition on the surface of the lithium metal. This is primarily due to the small pore size of the CPE membranes (~15 nm) in comparison with commercial PP separators (~25 nm), which facilitates blocking and restricts the migration of polysulfide molecules through the membranes. The polysulfide species, upon entering the highly porous CPE membranes are easily trapped in these nanopores, preventing further dissolution of the polysulfides. In addition, the extremely low E/S ratios (3:1 and 4:1 (mL g<sup>-1</sup>)) of the CPE membrane cells contrasted with Li–S cells containing liquid electrolyte with commercial separators (50:1 to 65:1 (mL g<sup>-1</sup>)) greatly restrict the mobility of polysulfides despite the high ionic conductivities. The result described herein is of significant value that will help initiate future research in GPE systems to be conducted focused on preventing polysulfide dissolution and dendrite formation in metallic lithium anodes using CPE separators.

#### ■ ASSOCIATED CONTENT

##### Supporting Information

The Supporting Information is available free of charge on the ACS Publications website at DOI: 10.1021/acsam.7b00094.

XRD patterns, SEM, FTIR spectra, results of flame tests, electrolyte uptake of the CPEs, and electrochemical charge–discharge profiles (PDF)

#### ■ AUTHOR INFORMATION

##### Corresponding Author

\*E-mail: [pkumta@pitt.edu](mailto:pkumta@pitt.edu).

##### ORCID

Prashant N. Kumta: 0000-0003-1227-1249

##### Notes

The authors declare no competing financial interest.

#### ■ ACKNOWLEDGMENTS

We acknowledge the financial support of U.S. Department of Energy (DOE) Grant DE-EE 000682S, Edward R. Weidlein Chair Professorship funds, and the Center for Complex Engineered Multifunctional Materials (CCEMM). P.N.K. also acknowledges support of the National Science Foundation, CBET-Grant 0933141 and CBET-Grant 1511390 for partial support of this research.

#### ■ REFERENCES

- (1) Song, D.; Ikuta, H.; Uchida, T.; Wakihara, M. The Spinel Phases LiAl<sub>y</sub>Mn<sub>2-y</sub>O<sub>4</sub> (y=0, 1/12, 1/9, 1/6, 1/3) and Li(Al,M)1/6Mn11/6O<sub>4</sub> (M=Cr, Co) as the Cathode for Rechargeable Lithium Batteries. *Solid State Ionics* **1999**, *117*, 151–156.
- (2) Kang, B.; Ceder, G. Battery Materials for Ultrafast Charging and Discharging. *Nature* **2009**, *458*, 190–193.
- (3) Croce, F.; Appetecchi, G. B.; Persi, L.; Scrosati, B. Nano-composite Polymer Electrolytes for Lithium Batteries. *Nature* **1998**, *394*, 456–458.
- (4) Manuel Stephan, A.; Nahm, K. S. Review on Composite Polymer Electrolytes for Lithium Batteries. *Polymer* **2006**, *47*, 5952–5964.
- (5) Whittingham, M. S. Lithium Batteries and Cathode Materials. *Chem. Rev.* **2004**, *104*, 4271–4302.
- (6) Sun, Y.-K.; Myung, S.-T.; Park, B.-C.; Prakash, J.; Belharouak, I.; Amine, K. High-Energy Cathode Material for Long-Life and Safe Lithium Batteries. *Nat. Mater.* **2009**, *8*, 320–324.
- (7) Tischer, R.; Ludwig, F. The Sulfur Electrode in Nonaqueous Media. *Adv. Electrochem. Electrochem. Eng.* **1977**, *10*, 391–482.
- (8) Yamin, H.; Peled, E. Electrochemistry of a Nonaqueous Lithium/Sulfur Cell. *J. Power Sources* **1983**, *9*, 281–287.
- (9) Marmorstein, D.; Yu, T. H.; Striebel, K. A.; McLarnon, F. R.; Hou, J.; Cairns, E. J. Electrochemical Performance of Lithium/Sulfur Cells with Three Different Polymer Electrolytes. *J. Power Sources* **2000**, *89*, 219–226.
- (10) Kolosnitsyn, V. S.; Karaseva, E. V. Lithium-Sulfur Batteries: Problems and Solutions. *Russ. J. Electrochem.* **2008**, *44*, 506–509.
- (11) Zhang, S. S. Liquid Electrolyte Lithium/Sulfur Battery: Fundamental Chemistry, Problems, and Solutions. *J. Power Sources* **2013**, *231*, 153–162.
- (12) Wang, J.; Chew, S. Y.; Zhao, Z. W.; Ashraf, S.; Wexler, D.; Chen, J.; Ng, S. H.; Chou, S. L.; Liu, H. K. Sulfur–Mesoporous Carbon Composites in Conjunction with a Novel Ionic Liquid Electrolyte for Lithium Rechargeable Batteries. *Carbon* **2008**, *46*, 229–235.
- (13) Yuan, L.; Yuan, H.; Qiu, X.; Chen, L.; Zhu, W. Improvement of Cycle Property of Sulfur-Coated Multi-Walled Carbon Nanotubes Composite Cathode for Lithium/Sulfur Batteries. *J. Power Sources* **2009**, *189*, 1141–1146.
- (14) Zheng, W.; Liu, Y. W.; Hu, X. G.; Zhang, C. F. Novel Nanosized Adsorbing Sulfur Composite Cathode Materials for the Advanced Secondary Lithium Batteries. *Electrochim. Acta* **2006**, *51*, 1330–1335.
- (15) Han, S.-C.; Song, M.-S.; Lee, H.; Kim, H.-S.; Ahn, H.-J.; Lee, J.-Y. Effect of Multiwalled Carbon Nanotubes on Electrochemical Properties of Lithium/Sulfur Rechargeable Batteries. *J. Electrochem. Soc.* **2003**, *150*, A889–A893.
- (16) Sun, M.; Zhang, S.; Jiang, T.; Zhang, L.; Yu, J. Nano-Wire Networks of Sulfur–Polypyrrole Composite Cathode Materials for Rechargeable Lithium Batteries. *Electrochem. Commun.* **2008**, *10*, 1819–1822.
- (17) Wang, J.; Chen, J.; Konstantinov, K.; Zhao, L.; Ng, S. H.; Wang, G. X.; Guo, Z. P.; Liu, H. K. Sulphur-Polypyrrole Composite Positive Electrode Materials for Rechargeable Lithium Batteries. *Electrochim. Acta* **2006**, *51*, 4634–4638.
- (18) Wang, J.; Yang, J.; Wan, C.; Du, K.; Xie, J.; Xu, N. Sulfur Composite Cathode Materials for Rechargeable Lithium Batteries. *Adv. Funct. Mater.* **2003**, *13*, 487–492.
- (19) Hanumantha, P. J.; Gattu, B.; Shanthi, P. M.; Damle, S. S.; Basson, Z.; Bandi, R.; Datta, M. K.; Park, S.; Kumta, P. N. Flexible

Sulfur Wires (Flex-Sws)—a New Versatile Platform for Lithium-Sulfur Batteries. *Electrochim. Acta* **2016**, *212*, 286–293.

(20) Liang, X.; Kwok, C. Y.; Lodi-Marzano, F.; Pang, Q.; Cuisinier, M.; Huang, H.; Hart, C. J.; Houtarde, D.; Kaup, K.; Sommer, H.; Brezesinski, T.; Janek, J.; Nazar, L. F. Tuning Transition Metal Oxide–Sulfur Interactions for Long Life Lithium Sulfur Batteries: The “Goldilocks” Principle. *Adv. Energy Mater.* **2016**, *6*, 1501636.

(21) Tao, X.; Wang, J.; Liu, C.; Wang, H.; Yao, H.; Zheng, G.; Seh, Z. W.; Cai, Q.; Li, W.; Zhou, G.; Zu, C.; Cui, Y. Balancing Surface Adsorption and Diffusion of Lithium-Polysulfides on Nonconductive Oxides for Lithium–Sulfur Battery Design. *Nat. Commun.* **2016**, *7*, 11203.

(22) Li, X.; Cao, Y.; Qi, W.; Saraf, L. V.; Xiao, J.; Nie, Z.; Mietek, J.; Zhang, J.-G.; Schwenzler, B.; Liu, J. Optimization of Mesoporous Carbon Structures for Lithium-Sulfur Battery Applications. *J. Mater. Chem.* **2011**, *21*, 16603–16610.

(23) Jin, J.; Wen, Z.; Ma, G.; Lu, Y.; Rui, K. Mesoporous Carbon/Sulfur Composite with Polyaniline Coating for Lithium Sulfur Batteries. *Solid State Ionics* **2014**, *262*, 170–173.

(24) Gong, Z.; Wu, Q.; Wang, F.; Li, X.; Fan, X.; Yang, H.; Luo, Z. A Hierarchical Micro/Mesoporous Carbon Fiber/Sulfur Composite for High-Performance Lithium-Sulfur Batteries. *RSC Adv.* **2016**, *6*, 37443–37451.

(25) Shanthi, P. M.; Hanumantha, P. J.; Gattu, B.; Sweeney, M.; Datta, M. K.; Kumta, P. N. Understanding the Origin of Irreversible Capacity Loss in Non-Carbonized Carbonate – Based Metal Organic Framework (Mof) Sulfur Hosts for Lithium – Sulfur Battery. *Electrochim. Acta* **2017**, *229*, 208–218.

(26) Hanumantha, P. J.; Gattu, B.; Velikokhatnyi, O.; Datta, M. K.; Damle, S. S.; Kumta, P. N. Heterostructures for Improved Stability of Lithium Sulfur Batteries. *J. Electrochem. Soc.* **2014**, *161*, A1173–A1180.

(27) Park, J.-W.; Ueno, K.; Tachikawa, N.; Dokko, K.; Watanabe, M. Ionic Liquid Electrolytes for Lithium–Sulfur Batteries. *J. Phys. Chem. C* **2013**, *117*, 20531–20541.

(28) Wang, L.; Liu, J.; Yuan, S.; Wang, Y.; Xia, Y. To Mitigate Self-Discharge of Lithium-Sulfur Batteries by Optimizing Ionic Liquid Electrolytes. *Energy Environ. Sci.* **2016**, *9*, 224–231.

(29) Zheng, J.; Gu, M.; Chen, H.; Meduri, P.; Engelhard, M. H.; Zhang, J.-G.; Liu, J.; Xiao, J. Ionic Liquid-Enhanced Solid State Electrolyte Interface (Sei) for Lithium-Sulfur Batteries. *J. Mater. Chem. A* **2013**, *1*, 8464–8470.

(30) Jeddi, K.; Sarikhani, K.; Qazvini, N. T.; Chen, P. Stabilizing Lithium/Sulfur Batteries by a Composite Polymer Electrolyte Containing Mesoporous Silica Particles. *J. Power Sources* **2014**, *245*, 656–662.

(31) Lin, Y.; Li, J.; Liu, K.; Liu, Y.; Liu, J.; Wang, X. Unique Starch Polymer Electrolyte for High Capacity All-Solid-State Lithium Sulfur Battery. *Green Chem.* **2016**, *18*, 3796–3803.

(32) Liu, M.; Zhou, D.; He, Y.-B.; Fu, Y.; Qin, X.; Miao, C.; Du, H.; Li, B.; Yang, Q.-H.; Lin, Z.; Zhao, T. S.; Kang, F. Novel Gel Polymer Electrolyte for High-Performance Lithium–Sulfur Batteries. *Nano Energy* **2016**, *22*, 278–289.

(33) Sun, Y.; Li, G.; Lai, Y.; Zeng, D.; Cheng, H. High Rate Lithium-Sulfur Battery Enabled by Sandwiched Single Ion Conducting Polymer Electrolyte. *Sci. Rep.* **2016**, *6*, 22048.

(34) Li, Y.; Xu, B.; Xu, H.; Duan, H.; Lü, X.; Xin, S.; Zhou, W.; Xue, L.; Fu, G.; Manthiram, A.; Goodenough, J. B. Hybrid Polymer/Garnet Electrolyte with a Small Interfacial Resistance for Lithium-Ion Batteries. *Angew. Chem.* **2017**, *129*, 771–774.

(35) Zhou, W.; Li, Y.; Xin, S.; Goodenough, J. B. Rechargeable Sulfur All-Solid-State Battery. *ACS Cent. Sci.* **2017**, *3*, 52–57.

(36) Aono, H.; Sugimoto, E.; Sadaoka, Y.; Imanaka, N.; Adachi, G. y. Ionic Conductivity of Solid Electrolytes Based on Lithium Titanium Phosphate. *J. Electrochem. Soc.* **1990**, *137*, 1023–1027.

(37) Li, J.; Ma, C.; Chi, M.; Liang, C.; Dudney, N. J. Solid Electrolyte: The Key for High-Voltage Lithium Batteries. *Adv. Energy Mater.* **2015**, *5*, 1401408.

(38) Kharton, V. V.; Marques, F. M. B.; Atkinson, A. Transport Properties of Solid Oxide Electrolyte Ceramics: A Brief Review. *Solid State Ionics* **2004**, *174*, 135–149.

(39) Rao, M.; Geng, X.; Li, X.; Hu, S.; Li, W. Lithium-Sulfur Cell with Combining Carbon Nanofibers–Sulfur Cathode and Gel Polymer Electrolyte. *J. Power Sources* **2012**, *212*, 179–185.

(40) Manuel Stephan, A. Review on Gel Polymer Electrolytes for Lithium Batteries. *Eur. Polym. J.* **2006**, *42*, 21–42.

(41) Fergus, J. W. Ceramic and Polymeric Solid Electrolytes for Lithium-Ion Batteries. *J. Power Sources* **2010**, *195*, 4554–4569.

(42) Gopalan, A. I.; Santhosh, P.; Manesh, K. M.; Nho, J. H.; Kim, S. H.; Hwang, C.-G.; Lee, K.-P. Development of Electrospun PvdF–Pan Membrane-Based Polymer Electrolytes for Lithium Batteries. *J. Membr. Sci.* **2008**, *325*, 683–690.

(43) Shalu; Singh, V. K.; Singh, R. K. Development of Ion Conducting Polymer Gel Electrolyte Membranes Based on Polymer PvdF-Hfp, Bmimtsfi Ionic Liquid and the Li-Salt with Improved Electrical, Thermal and Structural Properties. *J. Mater. Chem. C* **2015**, *3*, 7305–7318.

(44) Kim, J. R.; Choi, S. W.; Jo, S. M.; Lee, W. S.; Kim, B. C. Electrospun PvdF-Based Fibrous Polymer Electrolytes for Lithium Ion Polymer Batteries. *Electrochim. Acta* **2004**, *50*, 69–75.

(45) Agrawal, R. C.; Pandey, G. P. Solid Polymer Electrolytes: Materials Designing and All-Solid-State Battery Applications: An Overview. *J. Phys. D: Appl. Phys.* **2008**, *41*, 223001.

(46) Murata, K.; Izuchi, S.; Yoshihisa, Y. An Overview of the Research and Development of Solid Polymer Electrolyte Batteries. *Electrochim. Acta* **2000**, *45*, 1501–1508.

(47) Rao, M.; Geng, X.; Liao, Y.; Hu, S.; Li, W. Preparation and Performance of Gel Polymer Electrolyte Based on Electrospun Polymer Membrane and Ionic Liquid for Lithium Ion Battery. *J. Membr. Sci.* **2012**, *399–400*, 37–42.

(48) Idris, N. H.; Rahman, M. M.; Wang, J.-Z.; Liu, H.-K. Microporous Gel Polymer Electrolytes for Lithium Rechargeable Battery Application. *J. Power Sources* **2012**, *201*, 294–300.

(49) Gray, F. M. *Polymer Electrolytes*; Royal Society of Chemistry: London, 1997.

(50) MacCallum, J.; Vincent, C. *Polymer Electrolyte Reviews, Vol. 1*; Elsevier: London, 1989.

(51) MacCallum, J. R.; Vincent, C. A. *Polymer Electrolyte Reviews*; Springer Science & Business Media: Berlin, 1989; Vol. 2.

(52) Scrosati, B. *Applications of Electroactive Polymers*; Springer: Dordrecht, The Netherlands, 1993.

(53) Kim, K. M.; Park, N.-G.; Ryu, K. S.; Chang, S. H. Characteristics of PvdF-Hfp/Tio<sub>2</sub> Composite Membrane Electrolytes Prepared by Phase Inversion and Conventional Casting Methods. *Electrochim. Acta* **2006**, *51*, S636–S644.

(54) Adam, D. A Fine Set of Threads. *Nature* **2001**, *411*, 236–236.

(55) Manesh, K. M.; Kim, H. T.; Santhosh, P.; Gopalan, A. I.; Lee, K.-P. A Novel Glucose Biosensor Based on Immobilization of Glucose Oxidase into Multiwall Carbon Nanotubes–Polyelectrolyte-Loaded Electrospun Nanofibrous Membrane. *Biosens. Bioelectron.* **2008**, *23*, 771–779.

(56) Kim, H. S.; Jin, H.-J.; Myung, S. J.; Kang, M.; Chin, I.-J. Carbon Nanotube-Adsorbed Electrospun Nanofibrous Membranes of Nylon 6. *Macromol. Rapid Commun.* **2006**, *27*, 146–151.

(57) Huang, X.; Zeng, S.; Liu, J.; He, T.; Sun, L.; Xu, D.; Yu, X.; Luo, Y.; Zhou, W.; Wu, J. High-Performance Electrospun Poly(Vinylidene Fluoride)/Poly(Propylene Carbonate) Gel Polymer Electrolyte for Lithium-Ion Batteries. *J. Phys. Chem. C* **2015**, *119*, 27882–27891.

(58) Li, X.; Cheruvally, G.; Kim, J.-K.; Choi, J.-W.; Ahn, J.-H.; Kim, K.-W.; Ahn, H.-J. Polymer Electrolytes Based on an Electrospun Poly(Vinylidene Fluoride-Co-Hexafluoropropylene) Membrane for Lithium Batteries. *J. Power Sources* **2007**, *167*, 491–498.

(59) Rao, K. S.; El-Hami, K.; Kodaki, T.; Matsushige, K.; Makino, K. A Novel Method for Synthesis of Silica Nanoparticles. *J. Colloid Interface Sci.* **2005**, *289*, 125–131.

(60) Chen, X.; Mao, S. S. Synthesis of Titanium Dioxide (Tio<sub>2</sub>) Nanomaterials. *J. Nanosci. Nanotechnol.* **2006**, *6*, 906–925.

- (61) Nishiwaki, K.; Kakuta, N.; Ueno, A.; Nakabayashi, H. Generation of Acid Sites on Finely Divided TiO<sub>2</sub>. *J. Catal.* **1989**, *118*, 498–501.
- (62) Zhou, Z. Q.; Xu, H. Y.; Ji, W. J.; Chen, Y. Preparation of Novel Composite Vpo/Fumed Silica Catalyst for Partial Oxidation of N-Butane. *Catal. Lett.* **2004**, *96*, 221–226.
- (63) Kumar, B.; Scanlon, L. G. Polymer-Ceramic Composite Electrolytes. *J. Power Sources* **1994**, *52*, 261–268.
- (64) Manuel Stephan, A.; Teeters, D. Characterization of PvdF-Hfp Polymer Membranes Prepared by Phase Inversion Techniques I. Morphology and Charge–Discharge Studies. *Electrochim. Acta* **2003**, *48*, 2143–2148.
- (65) Song, J. Y.; Wang, Y. Y.; Wan, C. C. Conductivity Study of Porous Plasticized Polymer Electrolytes Based on Poly(Vinylidene Fluoride) a Comparison with Polypropylene Separators. *J. Electrochem. Soc.* **2000**, *147*, 3219–3225.
- (66) Li, L.; Jiang, Z.; Li, M.; Li, R.; Fang, T. Hierarchically Structured Pmma Fibers Fabricated by Electrospinning. *RSC Adv.* **2014**, *4*, 52973–52985.
- (67) Sethupathy, M.; Sethuraman, V.; Manisankar, P. Preparation of PvdF/SiO<sub>2</sub> Composite Nanofiber Membrane Using Electrospinning for Polymer Electrolyte Analysis. *Soft Nanosci. Lett.* **2013**, *3*, 29657.
- (68) Zhou, R.; Liu, W.; Yao, X.; Leong, Y. W.; Lu, X. Poly(Vinylidene Fluoride) Nanofibrous Mats with Covalently Attached SiO<sub>2</sub> Nanoparticles as an Ionic Liquid Host: Enhanced Ion Transport for Electrochromic Devices and Lithium-Ion Batteries. *J. Mater. Chem. A* **2015**, *3*, 16040–16049.
- (69) Solarajan, A. K.; Murugadoss, V.; Angaiah, S. High Performance Electrospun PVdF-HFP/SiO<sub>2</sub> Nanocomposite Membrane Electrolyte for Li-Ion Capacitors. *J. Appl. Polym. Sci.* **2017**, *134*, 45177.
- (70) Stephan, A. M.; Nahm, K. S.; Anbu Kulandainathan, M.; Ravi, G.; Wilson, J. Poly(Vinylidene Fluoride-Hexafluoropropylene) (PvdF-Hfp) Based Composite Electrolytes for Lithium Batteries. *Eur. Polym. J.* **2006**, *42*, 1728–1734.
- (71) Solarajan, A. K.; Murugadoss, V.; Angaiah, S. Dimensional Stability and Electrochemical Behaviour of ZrO<sub>2</sub> Incorporated Electrospun PvdF-Hfp Based Nanocomposite Polymer Membrane Electrolyte for Li-Ion Capacitors. *Sci. Rep.* **2017**, *7*, 45390.
- (72) Ding, Y.; Zhang, P.; Long, Z.; Jiang, Y.; Xu, F.; Di, W. The Ionic Conductivity and Mechanical Property of Electrospun P(VdF-Hfp)/Pmma Membranes for Lithium Ion Batteries. *J. Membr. Sci.* **2009**, *329*, 56–59.
- (73) Li, N.; Xiao, C.; An, S.; Hu, X. Preparation and Properties of PvdF/Pva Hollow Fiber Membranes. *Desalination* **2010**, *250*, 530–537.
- (74) Koganti, V. R.; Das, S.; Rankin, S. E. In Situ Ftir Investigation of the Kinetics of Silica Polycondensation in Surfactant Templated, Mesostructured Thin Films. *J. Phys. Chem. C* **2014**, *118*, 19450–19461.
- (75) Prabakaran, K.; Mohanty, S.; Nayak, S. K. Improved Electrochemical and Photovoltaic Performance of Dye Sensitized Solar Cells Based on Peo/PvdF-Hfp/Silane Modified Tio<sub>2</sub> Electrolytes and Mwcnt/Nafion[Registered Sign] Counter Electrode. *RSC Adv.* **2015**, *5*, 40491–40504.
- (76) Liao, L.-F.; Lien, C.-F.; Shieh, D.-L.; Chen, F.-C.; Lin, J.-L. Ftir Study of Adsorption and Photochemistry of Amide on Powdered Tio<sub>2</sub>: Comparison of Benzamide with Acetamide. *Phys. Chem. Chem. Phys.* **2002**, *4*, 4584–4589.
- (77) Feuillade, G.; Perche, P. Ion-Conductive Macromolecular Gels and Membranes for Solid Lithium Cells. *J. Appl. Electrochem.* **1975**, *5*, 63–69.
- (78) Blond, D.; Walshe, W.; Young, K.; Blighe, F. M.; Khan, U.; Almecija, D.; Carpenter, L.; McCauley, J.; Blau, W. J.; Coleman, J. N. Strong, Tough, Electrospun Polymer–Nanotube Composite Membranes with Extremely Low Density. *Adv. Funct. Mater.* **2008**, *18*, 2618–2624.
- (79) Matsumoto, K.; Sogabe, S.; Endo, T. Conductive Networked Polymer Gel Electrolytes Composed of Poly(Meth)Acrylate, Lithium Salt, and Ionic Liquid. *J. Polym. Sci., Part A: Polym. Chem.* **2012**, *50*, 1317–1324.
- (80) Li, W.; Pang, Y.; Liu, J.; Liu, G.; Wang, Y.; Xia, Y. A Peo-Based Gel Polymer Electrolyte for Lithium Ion Batteries. *RSC Adv.* **2017**, *7*, 23494–23501.
- (81) Tang, X.; Cao, Q.; Wang, X.; Peng, X.; Zeng, J. Study of the Effect of a Novel High-Performance Gel Polymer Electrolyte Based on Thermoplastic Polyurethane/Poly(Vinylidene Fluoride)/Polystyrene and Formed Using an Electrospinning Technique. *RSC Adv.* **2015**, *5*, 58655–58662.
- (82) Zhang, H.; Wang, X.; Liang, Y. Preparation and Characterization of a Lithium-Ion Battery Separator from Cellulose Nanofibers. *Heliyon* **2015**, *1*, No. e00032.
- (83) Perera, K.; Dissanayake, M. A. K. L.; Bandaranayake, P. W. S. K. Ionic Conductivity of a Gel Polymer Electrolyte Based on Mg(ClO<sub>4</sub>)<sub>2</sub> and Polyacrylonitrile (Pan). *Mater. Res. Bull.* **2004**, *39*, 1745–1751.
- (84) Zhang, R.; Chen, Y.; Montazami, R. Ionic Liquid-Doped Gel Polymer Electrolyte for Flexible Lithium-Ion Polymer Batteries. *Materials* **2015**, *8*, 2735.
- (85) Song, J. Y.; Wang, Y. Y.; Wan, C. C. Review of Gel-Type Polymer Electrolytes for Lithium-Ion Batteries. *J. Power Sources* **1999**, *77*, 183–197.
- (86) Huang, J.-Q.; Zhang, Q.; Peng, H.-J.; Liu, X.-Y.; Qian, W.-Z.; Wei, F. Ionic Shield for Polysulfides Towards Highly-Stable Lithium-Sulfur Batteries. *Energy Environ. Sci.* **2014**, *7*, 347–353.
- (87) Ma, G.; Huang, F.; Wen, Z.; Wang, Q.; Hong, X.; Jin, J.; Wu, X. Enhanced Performance of Lithium Sulfur Batteries with Conductive Polymer Modified Separators. *J. Mater. Chem. A* **2016**, *4*, 16968–16974.
- (88) Capuano, F.; Croce, F.; Scrosati, B. Composite Polymer Electrolytes. *J. Electrochem. Soc.* **1991**, *138*, 1918–1922.
- (89) Mohamed, N. S.; Arof, A. K. Conductivity Studies of Lic<sub>3</sub>so<sub>3</sub>-Doped and Dmf-Plasticized PvdF-Based Solid Polymer Electrolytes. *physica status solidi (a)* **2004**, *201*, 3096–3101.
- (90) Tanzi, M. C.; Mantovani, D.; Petrini, P.; Guidoin, R.; Laroche, G. Chemical Stability of Polyether Urethanes Versus Polycarbonate Urethanes. *J. Biomed. Mater. Res.* **1997**, *36*, 550–559.
- (91) Mihály, J.; Sterkel, S.; Ortner, H. M.; Kocsis, L.; Hajba, L.; Furdya, É.; Mink, J. Ftir and Ft-Raman Spectroscopic Study on Polymer Based High Pressure Digestion Vessels. *Croat. Chem. Acta* **2006**, *79*, 497–501.
- (92) Poliskie, M.; Clevenger, J. O. Fourier Transform Infrared (Ftir) Spectroscopy for Coating Characterization and Failure Analysis. *Met. Finish.* **2008**, *106*, 44–47.
- (93) Cui, C.; Park, D. H.; Kim, J.; Joo, J.; Ahn, D. J. Oligonucleotide Assisted Light-Emitting Alq<sub>3</sub>Microrods: Energy Transfer Effect with Fluorescent Dyes. *Chem. Commun.* **2013**, *49*, 5360–5362.
- (94) Prabavathi, N.; Senthil Nayaki, N.; Krishnakumar, V. Spectroscopic Investigation (FT-IR, FT-Raman, NMR and UV-Vis), Conformational Stability, NBO and Thermodynamic Analysis of 1-(2-Methoxyphenyl) Piperazine and 1-(2-Chlorophenyl) Piperazine by DFT Approach. *Pharm. Anal. Acta* **2015**, *6*, 391.
- (95) Ibrahim, M.; Nada, A.; Kamal, D. E. Density Functional Theory and Ftir Spectroscopic Study of Carboxyl Group. *Indian J. Pure Appl. Phys.* **2005**, *44*, 911–917.
- (96) Zhang, Z. P.; Rong, M. Z.; Zhang, M. Q.; Yuan, C. e. Alkoxyamine with Reduced Homolysis Temperature and Its Application in Repeated Autonomous Self-Healing of Stiff Polymers. *Polym. Chem.* **2013**, *4*, 4648–4654.
- (97) Saikia, B. J.; Parthasarathy, G. Fourier Transform Infrared Spectroscopic Characterization of Kaolinite from Assam and Meghalaya, Northeastern India. *J. Mod. Phys.* **2010**, *1*, 206–210.
- (98) El-Bahy, G. M. S. Ftir and Raman Spectroscopic Study of Fenugreek (*Trigonella Foenum Graecum* L.) Seeds. *J. Appl. Spectrosc.* **2005**, *72*, 111–116.
- (99) Sontevska, V.; Jovanovski, G.; Makreski, P.; Raškovska, A.; Šoptrajanova, B. Minerals from Macedonia. XXI. Vibrational Spectroscopy as Identificational Tool for Some Phyllosilicate Minerals. *Acta Chim. Slov.* **2008**, *55*, 757–766.
- (100) Biswas, N.; Waring, A. J.; Walther, F. J.; Dluhy, R. A. Structure and Conformation of the Disulfide Bond in Dimeric Lung Surfactant

Peptides Sp-B1–2S and Sp-B8–2S. *Biochim. Biophys. Acta, Biomembr.* **2007**, *1768*, 1070–1082.

(101) Park, K.; Cho, J. H.; Jang, J.-H.; Yu, B.-C.; De La Hoz, A. T.; Miller, K. M.; Ellison, C. J.; Goodenough, J. B. Trapping Lithium Polysulfides of a Li-S Battery by Forming Lithium Bonds in a Polymer Matrix. *Energy Environ. Sci.* **2015**, *8*, 2389–2395.